Journal of The Electrochemical Society, **161** (3) F360-F363 (2014)
0013-4651/2014/161(3)/F360/4/$31.00 © The Electrochemical Society

Evidence of Strong Metal-Support Interaction between Pt and Crystalline RuO_2 Nanosheets by In-Situ AFM

Qingfeng Liu, Christophe Chauvin,* and Wataru Sugimoto*,z

Materials and Chemical Engineering, Faculty of Textile Science and Technology, Shinshu University, Ueda, Nagano 386-8567, Japan

The enhancement in durability of Pt nanoparticles modified by nanostructured RuO_2 was studied using a model electrode consisting of vacuum deposited Pt on single crystalline RuO_2 nanosheets coated on highly oriented pyrolytic graphite (HOPG) surface with sub-monolayer coverage. Atomic force microscopy images showed that Pt on HOPG aggregated and tended to form 3-dimensional islands. On the other hand, Pt formed a well-defined, 2-dimensional over-layer on the RuO_2 nanosheet surface. In-situ atomic force microscopy images showed that deposited Pt on the HOPG surface readily dissolved and easily migrated with potential cycling in sulfuric acid, while no such phenomena could be observed on the RuO_2 nanosheets. The results indicate that RuO_2 nanosheet has a strong affinity toward Pt, namely strong metal-support interaction for Pt, which can be considered as one of the reasons for the enhanced durability of Pt/C modified by RuO_2 nanosheets.
 [DOI: 10.1149/2.106403jes]

Manuscript submitted November 8, 2013; revised manuscript received December 30, 2013. Published January 18, 2014.

Carbon supported Pt (Pt/C) is widely used as the cathode catalyst in polymer electrolyte fuel cells (PEFCs). The loss of the electrochemically active surface area due to the dissolution and coalescence of Pt nanoparticles during longtime operation is one of the major obstacles for wide-spread commercialization of PEFCs. Modifying Pt/C catalyst with oxides such as TiO_2,[1,2] SiO_2[3,4] or the use of SiO_2,[5] TiO_2,[6,7] WO_x,[8] SnO_2,[9] RuO_2[10–12] as corrosion-resistant support for Pt nanoparticles have been proposed to minimize the loss of activity. As an additive or support, it is desirable that the oxide phase is electrically conductive and stable in acidic environment. RuO_2 with electronic conductivity comparable to or higher than most carbonaceous materials, and with high resistance to corrosion seems to be an ideal material. Since RuO_2 is a precious metal oxide, it is essential that the oxide phase is used in a nanostructured form so as to reduce the content in catalyst. In addition, density functional theory has predicted that Pt grows in a 2-dimensional fashion due to the strong adsorption strength on RuO_2(110), suggesting that the presence of RuO_2 in the catalyst layer may enhance the activity for the oxygen reduction reaction.[12]

We have suggested the use of a highly crystalline RuO_2 nanomaterial, namely RuO_2 nanosheet[13] as an additive to enhance the properties of Pt-based electrocatalyts.[14–19] RuO_2 nanosheet is a 2-dimensional RuO_2 nanocrystal which is synthesized by chemical exfoliation of a layered ruthenic acid ($H_{0.2}RuO_{2.1} \cdot 0.9H_2O$).[13] The 2-dimensional nanosheet has high surface/bulk ratio due to the ultimately thin thickness of ~1 nm and retains the original properties of the bulk oxide such as excellent electronic/protonic conductivity and electrochemical stability. We have recently shown that the durability of commercial Pt supported on carbon black can be enhanced with the addition of RuO_2 nanosheet.[17,18] Model electrode studies have elucidated that there is a strong electrostatic interaction between RuO_2 nanosheets and dissolved Pt ions derived electrochemically.[19] This strong electrostatic interaction between ionic Pt species in solution and the nanosheets is considered to decrease the loss of dissolved Pt species into electrolyte due to migration.

In this study, we present experimental evidence of a strong metal-support interaction between RuO_2 nanosheet and metallic Pt, which may be another reason for the enhanced durability of RuO_2 nanosheet modified Pt/C. A model electrode system was employed to evaluate the difference in the adsorption strength of metallic Pt on RuO_2 nanosheet and carbon surfaces. Highly oriented pyrolytic graphite (HOPG) with a sub-monolayer coverage of RuO_2 nanosheet (RuO_2 nanosheet/HOPG) was prepared as model electrode, and Pt was vacuum deposited on its surface (Pt-RuO_2 nanosheet/HOPG). This allowed the characterization of the morphology of Pt on nanosheet and HOPG by atomic force microscopy (AFM) concurrently under the same conditions. In-situ electrochemical-atomic force microscopy (EC-AFM) measurements were performed to investigate the electrochemical behavior of Pt dissolution/re-deposition on the surface of nanosheet and HOPG during potential cycling.

Experimental

RuO_2 nanosheets were synthesized by elemental exfoliation of an ion-exchangeable layered potassium ruthenate ($K_{0.2}RuO_{2.1} \cdot nH_2O$) following our previous report.[20] Proton-exchange of the interlayer potassium was conducted with 1 mol dm^{-3} HCl for 3 days at 60°C, resulting in the layered ruthenic acid ($H_{0.2}RuO_{2.1} \cdot 0.9H_2O$). The layered ruthenic acid was added to an aqueous solution of tetrabutylammonium hydroxide (TBAOH) with the molar ratio of TBA ions to the exchangeable protons in $H_{0.2}RuO_{2.1} \cdot 0.9H_2O$ adjusted to $TBA^+/H^+ = 1.5$. The dispersion was vigorously shaken for 10 days to exfoliate $H_{0.2}RuO_{2.1} \cdot 0.9H_2O$ into elementary RuO_2 nanosheets. Non-exfoliated impurity was removed by centrifugation at 2000 rpm for 30 min. The as-exfoliated nanosheet colloid was finally diluted to 0.1 (g-RuO_2) L^{-1} with ultrapure water (Milli-Q, >18 MΩ cm). HOPG (Bruker, ZYH-grade, 12 × 12 mm^2) was freshly cleaved using adhesive tape and then immersed into this diluted nanosheet colloid for 2 minutes to coat RuO_2 nanosheet (RuO_2 nanosheet/HOPG). Pt was evaporated onto the surface of RuO_2 nanosheet/HOPG using a vacuum evaporation equipment (Shimadzu, E-250A). A Pt wire (Nilaco, 0.5 mm in diameter, 10 mm in length, 99.95%) acted as the evaporation source. The amount of Pt deposited (Ma = 0.22 × 10^{15} or 1.33 × 10^{15} atoms cm^{-2}) was monitored by a quartz thickness monitor (Anelva, INFICON SQM-160).

The surface of the model electrodes was characterized using an electrochemical-atomic force microscope (EC-AFM, Bruker, Digital Instruments Nanoscope III D ADC 5) equipped with a bi-potentiostat. Images were recorded using a SiN probe (Bruker, SNL-10). Cyclic voltammetry was performed from 0 to 1.2 V vs. RHE at a scan rate of 50 mV s^{-1} in a three-electrode electrochemical cell (Bruker, MultiMode) with 0.5 M H_2SO_4 as the electrolyte at room temperature in air (without de-aeration due to the small size of the EC-AFM cell). The model electrode acted as the working electrode and two high purity Pt wires with diameter of 0.5 mm and 0.1 mm acted as the reference and the counter electrodes, respectively. All the potentials in the paper have been converted to reversible hydrogen electrode (RHE) scale by adding 0.90 V to the values measured with the Pt quasi-reference electrode which was calibrated against a reversible hydrogen electrode. The geometric area of the working electrode in contact with the electrolyte was 0.5 cm^2. The time for acquiring an AFM image was approximately 5 minutes. All the AFM images were processed using Nanoscope V531r1 software.

*Electrochemical Society Active Member.
zE-mail: wsugi@shinshu-u.ac.jp

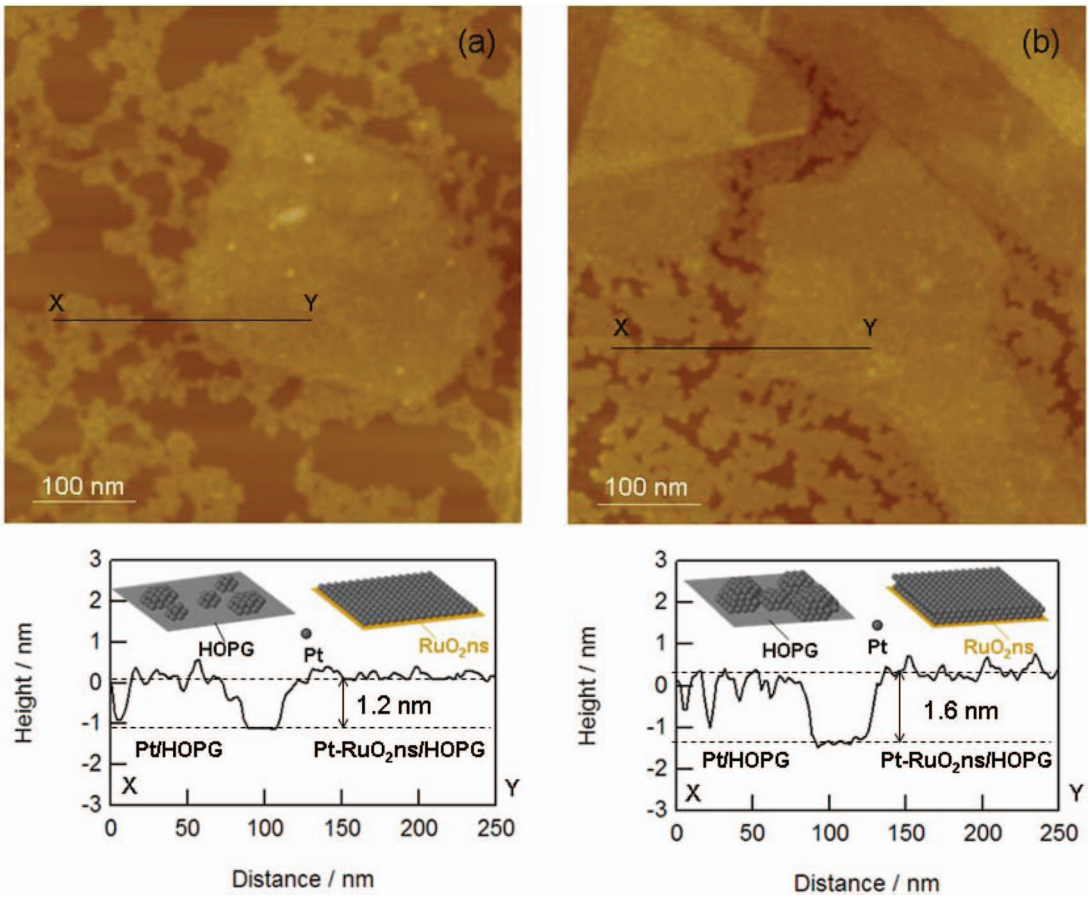

Figure 1. AFM topographic images (above) and height profiles from X to Y (below) of Pt-RuO_2 nanosheet/HOPG in air. The amount of deposited Pt (*M*a: atoms cm^{-2}) shown in (a) and (b) are 0.22×10^{15} and 1.33×10^{15} atoms cm^{-2}, respectively. The *z*-range is 10 nm.

Results and Discussion

Figure 1 shows typical AFM images and height profiles of RuO_2 nanosheet/HOPG model electrodes with different amounts of deposited Pt (Pt-RuO_2 nanosheet/HOPG), *M*a = 0.22×10^{15} and 1.33×10^{15} atoms cm^{-2}. On bare HOPG, The deposited Pt aggregates to form islands. On the contrary, Pt forms a well-defined over-layer on the nanosheets. For the model electrode with lower amount of Pt (*M*a = 0.22×10^{15} atoms cm^{-2}), the Pt islands on HOPG have a height of 1.1 ± 0.7 nm and the height of RuO_2 nanosheet covered with Pt is 1.2 ± 0.4 nm (Figure 1a). Since the thickness of RuO_2 nanosheet is 1.0 ± 0.1 nm,[19] the Pt over-layer should be ∼0.2 nm thick. Taking into account of the diameter of Pt atom as 0.28 nm, the Pt over-layer deposited on RuO_2 nanosheet is close to a thin continuous monolayer (ML) film. For the model electrode with more Pt (*M*a = 1.33×10^{15} atoms cm^{-2}), the height of Pt deposits on HOPG was 1.5 ± 0.8 nm (Figure 1b). The height of RuO_2 nanosheet with Pt over-layer was 1.6 ± 0.7 nm, thus the thickness of Pt over-layer should be ∼0.6 nm. This thickness is about twice the atomic diameter of Pt (0.28 nm), thus the Pt over-layer is considered as a 2 ML film. The 3-dimensional growth of Pt deposits on HOPG and 2-dimensional growth on RuO_2 nanosheet indicate two different film growth modes, namely Volmer-Weber growth (3-dimensional growth) and Frank-van der Merwe growth (2-dimensional growth).[21] The two different growth modes reveal that RuO_2 nanosheet has a stronger adsorption strength or affinity to Pt compared to HOPG. This is in good agreement with density functional theory calculations that predicted strong adsorption of Pt on RuO_2(100) leading to energetically favorable 2-dimensional growth of up to 1.25 ML.[12] RuO_2 nanosheet evidently has similar properties with bulk RuO_2.

Next, the electrochemical stability of Pt aggregated on HOPG (Pt/HOPG) compared to Pt on RuO_2 nanosheet (Pt/RuO_2 nanosheet) was studied by in-situ EC-AFM. Figure 2 shows a sequence of in-situ EC-AFM images and the respective height profiles of the Pt-RuO_2 nanosheet/HOPG model electrode (*M*a = 1.33×10^{15} atoms cm^{-2}) with potential cycling (0–1.2 V vs. RHE, 50 mV s^{-1}) in 0.5 M H_2SO_4 at room temperature. The topographic images clearly show that the amount of Pt on bare HOPG gradually decreases and more HOPG surface is exposed with increasing number of potential cycling. On the other hand, the maximum thickness of the Pt over-layers on nanosheets increases with potential cycling from ∼0.9 nm for the 10th cycle to ∼1.4 nm after 40 cycles as shown in the height profiles in Figure 2. This result can also be identified clearly from the comparison of the height profiles shown in Figure 3. This strong affinity of RuO_2 nanosheet with metallic Pt is an indication of the so-called strong metal-support interaction (SMSI) as found in oxides such as CeO_2[22] and TiO_2.[23,24] It is noted that the Pt deposit on HOPG shown in Figure 3 is moving to the right with potential cycling, which indicates that the deposited Pt on HOPG migrates easily; i.e. Pt nanoparticles have weak affinity to HOPG.

Figure 4 shows the cyclic voltammograms (CVs) of the Pt-RuO_2 nanosheet/HOPG model electrode in 0.5 M H_2SO_4 corresponding to Figure 2a–2d. The negative shift in currents observed below 0.8 V vs. RHE is due to oxygen reduction reaction, since measurements were conducted in atmospheric conditions. De-aeration of the electrolyte was difficult to conduct due to the small size of the EC-AFM cell. Distinctive peaks

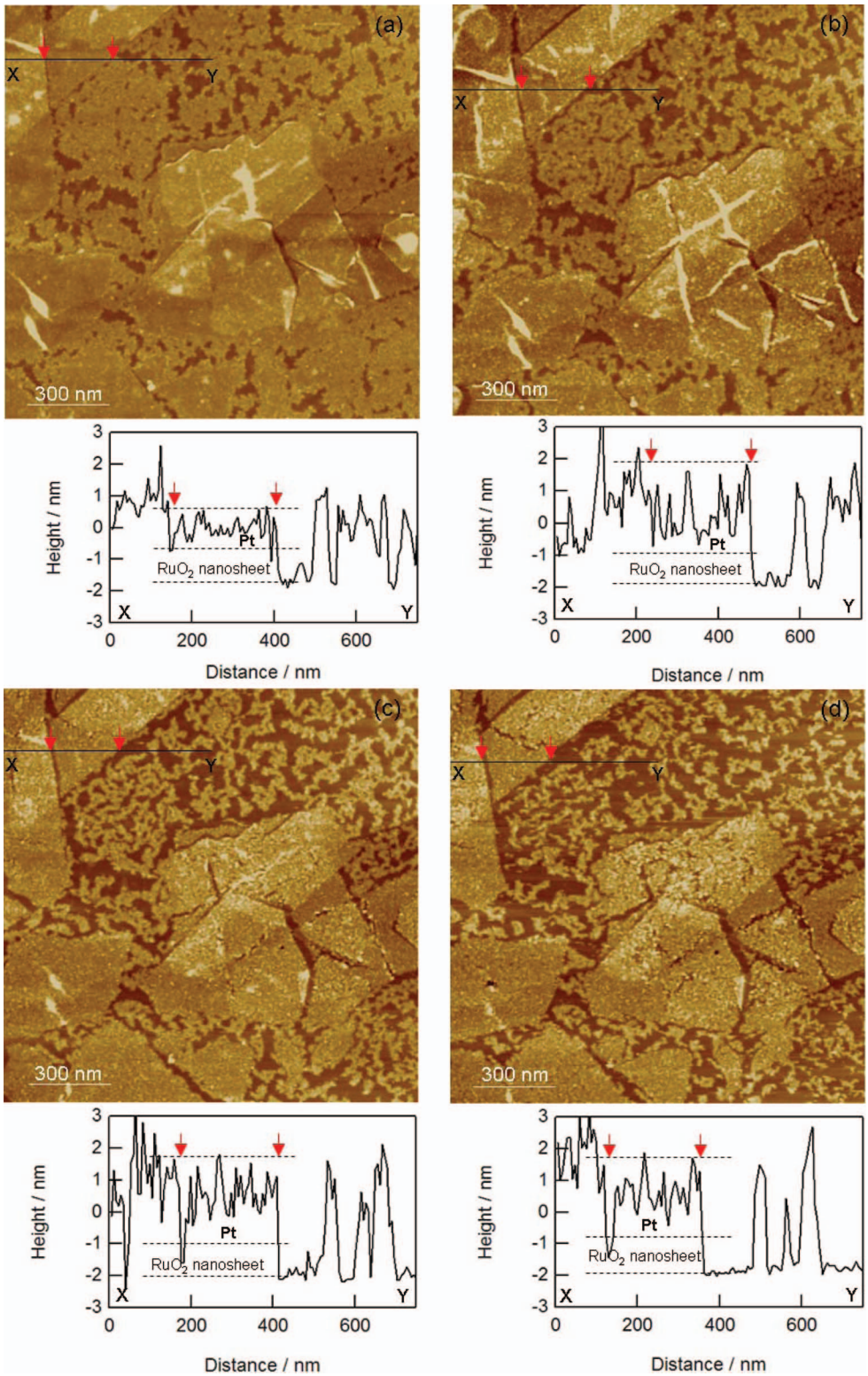

Figure 2. In situ EC-AFM topographic images and height profiles from X to Y in 0.5 M H_2SO_4 after potential cycling (from 0 to 1.2 V vs. RHE). a-d: after 10, 20, 30, 40 cycles. The z-range is 10 nm and $Ma = 1.33 \times 10^{15}$ atoms cm^{-2}.

attributed to surface redox process on RuO_2 nanosheet are observed at half wave potential of $E_{1/2} = 0.11$ and 0.62 V vs. RHE in the CVs. The redox pair at $E_{1/2} = 0.62$ V vs. RHE does not change, indicating the stability of the RuO_2 nanosheets with potential cycling. On the other hand, the current below 0.2 V decreases with potential cycling. The current observed in this region is due to double-layer charging, hydrogen adsorption/desorption on Pt, and pseudocapacitance of RuO_2 nanosheets. Since the RuO_2 nanosheets do not degrade, the decrease in current can be attributed to loss in electrochemical active surface area of Pt due to Pt dissolution or aggregation. This phenomenon can also be seen from the decrease in anodic current >1.0 V vs. RHE, which is related to the oxidation of Pt. It is assumed

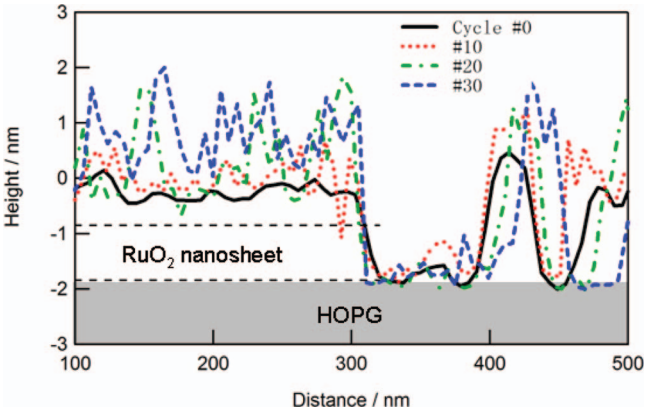

Figure 3. Comparison of the height profiles of initial, after 10, 20, and 30 cycles of AFM images in Figure 2.

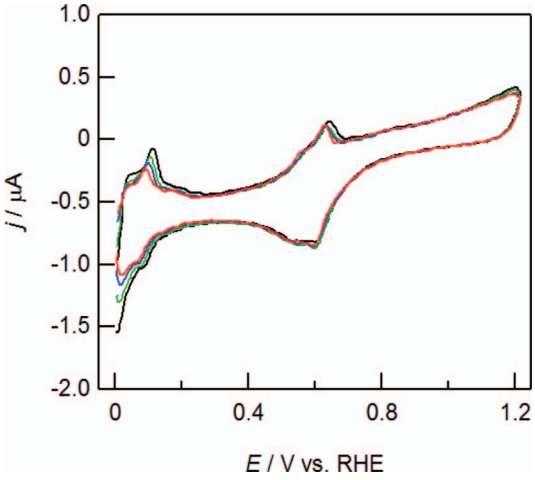

Figure 4. CVs (scan rate: 50 mV s^{-1}) recorded for Pt-RuO_2 nanosheet/HOPG in 0.5 M H_2SO_4 during in-situ EC-AFM measurements ($Ma = 1.33 \times 10^{15}$ atoms cm^{-2}). (black line: after 10 cycles, green line: after 20 cycles, blue line: after 30 cycles, red line: after 40 cycles).

that both Pt on HOPG and Pt on RuO_2 nanosheet/HOPG are active. Further model electrode studies with different RuO_2 nanosheet coverage should allow a more quantitative discussion on the degree of mitigation of Pt loss with RuO_2 nanosheets, and is presently under consideration.

Conclusions

Pt was vacuum deposited on model electrodes composed of HOPG partially covered with crystalline RuO_2 nanosheets to investigate the difference in the interaction between Pt with RuO_2 nanosheet or HOPG. AFM images show that on HOPG, Pt aggregates and forms 3-dimensional islands via Volmer-Weber growth, whereas Pt is deposited as a thin over-layer on the RuO_2 nanosheet surface via Frank-van der Merwe growth (2-dimensional growth). The two different growth modes reveal that Pt has a stronger adsorption strength or affinity to RuO_2 nanosheet compared to HOPG, i.e. strong metal-support interaction. In-situ EC-AFM experiments reveal that Pt nanoparticles on HOPG are more susceptible to electrochemical active surface area loss than the Pt over-layer on RuO_2 nanosheet. The results suggest that RuO_2 nanosheet supported Pt is likely to be a more stable catalyst than carbon supported Pt. RuO_2 nanosheet can be anticipated to play multiple roles in enhancing the durability of practical carbon supported Pt catalysts for polymer electrolyte fuel cells, including strong metal-support interaction, electrostatic interaction with dissolved Pt cations, and also as a stable oxide support.

Acknowledgments

This work was supported in part by the "Polymer Electrolyte Fuel Cell Program" from the New Energy and Industrial Technology Development Organization (NEDO), Japan and a grant in-Aid for Excellent Graduate Schools, of the Ministry of Education, Culture, Sports, Science and Technology (MEXT), Japan.

References

1. J. Tian, G. Sun, M. Cai, Q. Mao, and Q. Xin, *J. Electrochem. Soc.*, **155**, B187 (2008).
2. X. Liu, J. Chen, G. Liu, L. Zhang, H. Zhang, and B. Yi, *J. Power Sources*, **195**, 4098 (2010).
3. S. Takenaka, H. Matsumori, H. Matsune, E. Tanabe, and M. Kishida, *J. Electrochem. Soc.*, **155**, B929 (2008).
4. S. Takenaka, H. Matsumori, H. Matsune, and M. Kishida, *Appl. Catal., A*, **409-410**, 248 (2011).
5. B. Seger, A. Kongkanand, K. Vinodgopal, and P. V. Kamat, *J. Electroanal. Chem.*, **621**, 198 (2008).
6. M. Gustavsson, H. Ekström, P. Hanarp, L. Eurenius, G. Lindbergh, E. Olsson, and B. Kasemo, *J. Power Sources*, **163**, 671 (2007).
7. D.-S. Kim, E. F. A. Zeid, and Y.-T. Kim, *Electrochim. Acta*, **55**, 3628 (2010).
8. T. Ioroi, Z. Siroma, N. Fujiwara, S. Yamazaki, and K. Yasuda, *Electrochem. Commun.*, **7**, 183 (2005).
9. A. Masao, S. Noda, F. Takasaki, K. Ito, and K. Sasaki, *Electrochem. Solid-State Lett.*, **12**, B119 (2009).
10. C. P. Lo and V. Ramani, *ACS Appl. Mater. Interfaces*, **4**, 6109 (2012).
11. C. P. Lo, G. Wang, A. Kumar, and V. Ramani, *Appl. Catal., B*, **140–141**, 133 (2013).
12. P. Liu, J. T. Muckerman, and R. R. Adzic, *J. Chem. Phys.*, **124**, 141101 (2006).
13. W. Sugimoto, H. Iwata, Y. Yasunaga, Y. Murakami, and Y. Takasu, *Angew. Chem., Int. Ed.*, **42**, 4092 (2003).
14. W. Sugimoto, T. Saida, and Y. Takasu, *Electrochem. Commun.*, **8**, 411 (2006).
15. T. Saida, Y. Takasu, and W. Sugimoto, *Electrochemistry*, **79**, 371 (2011).
16. T. Saida, W. Sugimoto, and Y. Takasu, *Electrochim. Acta*, **55**, 857 (2010).
17. C. Chauvin, Q. Liu, T. Saida, K. S. Lokesh, T. Sakai, and W. Sugimoto, *ECS Trans.*, **50**(2), 1583 (2013).
18. D. Takimoto, C. Chauvin, and W. Sugimoto, *Electrochem. Commun.*, **33**, 123 (2013).
19. Q. Liu, K. S. Lokesh, C. Chauvin, and W. Sugimoto, *J. Electrochem. Soc.*, **161**, F259 (2014).
20. K. Fukuda, H. Kato, J. Sato, W. Sugimoto, and Y. Takasu, *J. Solid State Chem.*, **182**, 2997 (2009).
21. J. A. Venables, *Surf. Sci.*, **299**, 798 (1994).
22. G. N. Vayssilov, Y. Lykhach, A. Migani, T. Staudt, G. P. Petrova, N. Tsud, T. Skala, A. Bruix, F. Illas, K. C. Prince, V. Matolin, K. M. Neyman, and J. Libuda, *Nat. Mater.*, **10**, 310 (2011).
23. A. G. Dylla and K. J. Stevenson, *Chem. Commun.*, **47**, 12104 (2011).
24. A. B. Arjad and J. A. Yarmoff, *J. Phys. Chem. C*, **116**, 23377 (2012).